EPR study of local symmetry sites of Ce^{3+} in $Pb_{1-x}Ce_xA$ (A=S, Se, and Te)

X. Gratens, V. Bindilatti, V. A. Chitta, and N. F. Oliveira, Jr.
Instituto de Física, Universidade de São Paulo, C.P. 66.318, 05314-970 São Paulo, Brazil

S. Isber
Department of Physics, American University of Beirut, Bliss Street, P.O. Box 11-0236 Beirut, Lebanon

Z. Golacki
Institute of Physics, Polish Academy of Sciences, Pl. 02-668 Warsaw, Poland
(Received 17 October 2008; published 24 February 2009)

The local site symmetry of Ce^{3+} ions in the diluted magnetic semiconductors $Pb_{1-x}Ce_xA$ (A=S, Se, and Te) has been investigated by electron-paramagnetic resonance (EPR). The experiments were carried out on single crystals with cerium concentration x ranging from 0.001 to 0.035. The isotropic line due to Ce^{3+} ions located at the substitutional Pb cation site with octahedral symmetry was observed for all the studied samples. We determined the effective Landé factors to be g=1.333, 1.364, and 1.402 for A=S, Se, and Te, respectively. The small difference with the predicted Landé factor g of 10/7 for the Γ_7 (J=5/2) ground state was attributed to crystal-field admixture. In addition, EPR lines from Ce^{3+} ions located at sites with small distortion from the original octahedral symmetry were also observed. Two distinct sites with axial distortion along the ⟨001⟩ crystallographic direction were identified and a third signal in the spectrum was attributed to sites with the cubic symmetry distorted along the ⟨110⟩ direction. The distortion at these distinct Ce sites is attributed to Pb lattice vacancies near the cerium ions that compensate for its donor activity.

DOI: 10.1103/PhysRevB.79.075207 PACS number(s): 76.30.−v, 71.70.Gm

I. INTRODUCTION

In recent years, important efforts have been dedicated to the study of diluted magnetic semiconductors (DMSs).[1,2] These are semiconductors where a fraction of the original cations is substituted by magnetic ions. Lead salts compounds (PbS, PbSe, and PbTe) containing europium ions are well-known examples of IV-VI-based DMS. In $Pb_{1-x}Eu_xA$ (A=S, Se, and Te) europium ions (Eu^{2+}) enter the rocksalt structure of the lead salt replacing Pb^{2+}. Studies of IV-VI semiconductors doped with mixed valence (divalent and trivalent) rare-earth ions (Gd and Yb) have been also reported.[3–6] It was found that the existence of magnetically active states (trivalent ions) in the DMS is conditioned by the presence of native defects pushing out electrons from the nonmagnetic state (divalent). Recently, magnetic properties of lead salts containing Ce^{3+} ions have been investigated[7–9] by magnetization step studies.[10] The results showed the existence of two equally populated types of nearest-neighbor (nn) Ce^{3+} pairs coupled by antiferromagnetic exchange interactions having distinct properties. The first type was found to have an isotropic exchange interaction whereas the second type experiences properties which can be modeled by an anisotropic exchange interaction. The existence of these two distinct types of nn pairs is not yet well understood.

Unlike other multivalent rare-earth ions (such as Gd and Yb), the present study shows that cerium enters the lattice of the lead salts only in the trivalent Ce^{3+} state which should exhibit donorlike properties. Therefore, self-compensation phenomena[11–14] (i.e., a partial compensation of the cerium donor by acceptor activity from native point defects) may also occur in $Pb_{1-x}Ce_xA$. The predicted ground state for Ce^{3+} substituting Pb^{2+} (octahedral site symmetry) in the rocksalt structure of $Pb_{1-x}Ce_xA$ is the doublet Γ_7.[15] The presence of a point defect acting as compensator in the near vicinity of a magnetic ion may significantly affect its ground state by lowering the cubic symmetry at the Ce^{3+} site. This was experimentally confirmed in the present work by means of electron-paramagnetic-resonance (EPR) measurements and carrier density measurements for different cerium contents. Cerium has no magnetic isotopes and the EPR spectrum contains no hyperfine structure which could facilitate the detection and identification of the different types of Ce^{3+} sites. All the EPR signals reported here are due to single cerium ions that are not coupled by exchange interaction with other Ce^{3+} ions. Four types of Ce^{3+} substituting Pb^{2+} sites have been identified. The most populated type corresponds to octahedral cubic (O_h) site symmetry. The other types correspond to cubic sites slightly distorted along the ⟨001⟩ and ⟨110⟩ axes of the crystal.

II. EXPERIMENTAL

The studied samples ($0.001 \leq x \leq 0.035$) were single crystals ($1 \times 1 \times 2$ mm^3) grown by the Bridgman method. X-ray diffraction spectra exhibited the conventional peaks pattern for the rocksalt structure of lead salts. The Ce^{3+} concentration x was determined from magnetization measurements.[16] Similar values for x were also obtained from the fitting of magnetic susceptibility at low magnetic fields.[17] The EPR spectra were collected at 4.2 K using an X-band EPR spectrometer equipped with an Oxford Instrument helium gas flow cryostat. The He flow was directly injected onto the sample. The (001) cleavage planes of the crystal were used to orient the samples in the cavity. The external magnetic field (**H**) was rotated in the (100) plane. To improve the signal to noise ratio, several spectra were accumulated and

TABLE I. Single-ion Hamiltonian parameters for Ce^{3+} in the O_h site symmetry. The crystal-field parameters b_4 and b_6 as well as the crystal-field splitting Δ_{78} between the ground state Γ_7 and the next excited state Γ_8 are given in kelvin.

DMS	g	b_4/k_B	b_6/k_B	Δ_{78}/k_B
$Pb_{1-x}Ce_xTe$	1.400 ± 0.001	37 ± 1	-2.6 ± 0.8	340 ± 5
$Pb_{1-x}Ce_xSe$	1.361 ± 0.001	48 ± 0.5	-2.4 ± 0.1	440 ± 5
$Pb_{1-x}Ce_xS$	1.332 ± 0.001	58 ± 6	-2.2 ± 0.7	540 ± 5

averaged for each orientation of the external magnetic field.

III. EXPERIMENTAL RESULTS

A. Overall view

Microprobe measurements were performed on three samples of $Pb_{1-x}Ce_xSe$ (x=0.035, 0.020, and 0.016) and one sample of $Pb_{1-x}Ce_xS$ with x=0.020. The average concentrations of cerium atoms, determined from about 50 spots, were found to match those obtained from magnetic measurements. This result is strong evidence that cerium is present only as the magnetic Ce^{3+} in $Pb_{1-x}Ce_xA$. For the two other studied $Pb_{1-x}Ce_xTe$ samples, cerium concentrations were low enough to avoid crystal inhomogeneity observed in a previous work.[18]

Furthermore, the analysis of the magnetic-susceptibility data gave the following results: (i) The ground-state doublet Γ_7 is well separated from the next excited energy level (quadruplet Γ_8). The values of the crystal-field splitting Δ_{78} are given in Table I for the three DMSs. (ii) The data are consistent with the existence of weak antiferromagnetic exchange interactions (as expected) between Ce^{3+}. (iii) Magnetic-susceptibility data showed no signal traces due to any magnetic phase originating from CeS, CeSe, or CeTe clustering.

Hall-effect measurements performed on a few samples of $Pb_{1-x}Ce_xA$ showed that cerium has donorlike activity. Figures 1 and 2 show the EPR spectrum obtained at T=4.2 K with $\mathbf{H} \| [001]$ for the $Pb_{1-x}Ce_xTe$ sample with x=0.004 and the $Pb_{1-x}Ce_xSe$ sample with x=0.013, respectively. These are representative spectra of the $Pb_{1-x}Ce_xA$ samples series. The analysis of the EPR line positions and their relative intensities at various orientations of the external magnetic field allowed the identification of four distinct sites for Ce^{3+} substituting Pb^{2+}:

Signal I. The intense central isotropic line is due to Ce^{3+} ions located in sites with octahedral (O_h) symmetry (site I). This line was observed for all the eleven studied samples at T=4.2 K and for temperatures up to 100 K. The observed Dysonian line shape[19] is due to the high conductivity of the material. Signal I is the result of EPR transitions within the doublet Γ_7 ground state predicted for Ce^{3+} in O_h site symmetry. The g value was determined for all the samples using Dysonian line-shape analysis. We obtained $g = 1.332 \pm 0.002$, $g = 1.361 \pm 0.002$, and $g = 1.400 \pm 0.001$ for A=S, Se, and Te, respectively. These values are slightly different from the predicted $g = \frac{10}{7}$ of the doublet Γ_7. These differences are attributed to crystal-field admixture discussed in Sec. III B.

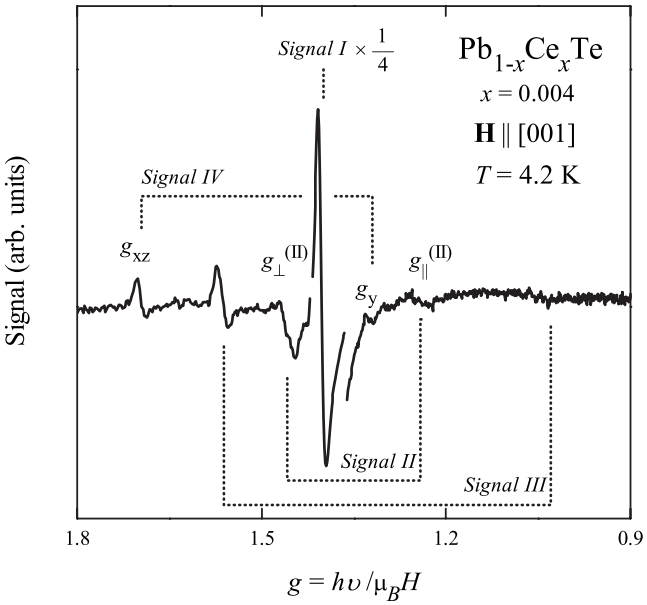

FIG. 1. EPR spectrum of $Pb_{1-x}Ce_xTe$ crystal with x=0.004. Signal I is due to Ce^{3+} ions with cubic (O_h) site symmetry. Its intensity was divided by 4 to emphasize the presence of the other lines. Signals II and III are due to Ce^{3+} ions with the original cubic site symmetry distorted along the ⟨001⟩ axis. Signal IV is attributed to cubic Ce sites distorted along the ⟨110⟩ direction.

Signal II. It consists of two lines around signal I and exhibits tetragonal symmetry due to a small axial distortion of the cubic site along one of the three ⟨001⟩ crystal axes.

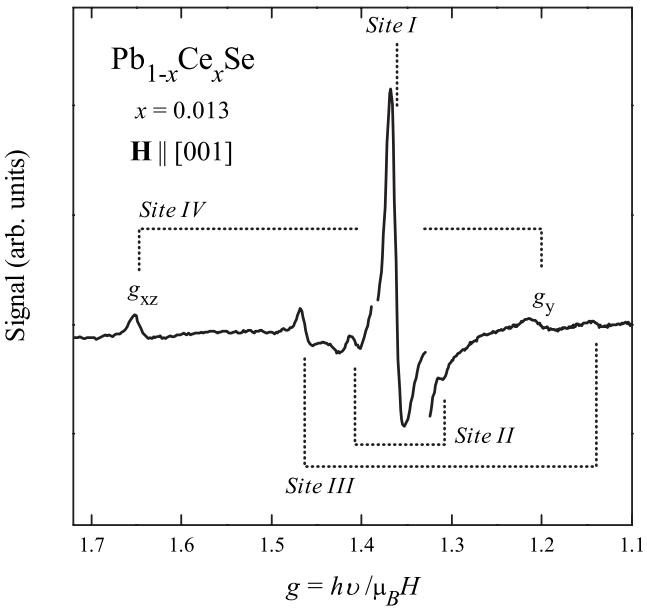

FIG. 2. EPR spectrum of $Pb_{1-x}Ce_xSe$ (x=0.013) crystal at T =4.2 K. The EPR signals from Ce^{3+} ions located into weakly distorted cubic site symmetry (sites II and III) are manifested around the central signal due to Ce^{3+} ions in an octahedral cubic environment (site I). The intensity of the central line (site I) was divided by 4 to emphasize the presence of the other lines.

TABLE II. g values of sites II and III for the three investigated DMSs. These values were used to determine the parameter b_2^0.

	Site II			Site III		
DMS	$g_\perp$	$g_\parallel$	b_2^0 (K)	$g_\perp$	$g_\parallel$	b_2^0/k_B (K)
X=Te	1.460	1.240	-1.6 ± 0.1	1.561	1.030	-3.8 ± 0.1
X=Se	1.407	1.308	-1.1 ± 0.1	1.463	1.145	-3.25 ± 0.05
X=S	1.359	1.263	-1.2 ± 0.1	1.405	1.163	-3.0 ± 0.05

This site is labeled site II. The line with larger intensity (to the left of signal I in Fig. 1) corresponds to site II whose distortion axes are perpendicular to the magnetic field $g_\perp^{(\mathrm{II})}$ whereas the broad line to the right of signal I is due to sites whose distortion axes are parallel to the magnetic field $g_\parallel^{(\mathrm{II})}$. The lines were clearly identified by analyzing their angular variations and relative intensities. The lines at $g_\perp$ and $g_\parallel$ have degeneracies of 2 and 1, respectively. By rotating the magnetic field in the (100) plane of the crystal one of the $g_\perp$ transitions remains at the same position. The other $g_\perp$ line and the $g_\parallel$ line are to be displaced in such manner that they exchange field positions when the rotation angle attains 90°.

Signal III. It is due to another tetragonal site (labeled site III) with a larger splitting $(g_\perp^{(\mathrm{III})}-g_\parallel^{(\mathrm{III})})$ than that of site II. The experimental g values for sites II and III are given in Table II for the three DMSs.

Signal IV. It consists of two lines marked in Fig. 1 as g_{xz} and g_y. This signal is tentatively attributed to a cubic site with a small distortion of the symmetry along one of the six $\langle 110\rangle$ directions of the crystal. This site is labeled here as site IV. In this case, the spectrum should exhibit an orthorhombic site symmetry which can be described by the effective g factors g_x, g_y, and g_z with the z axis along $\langle 110\rangle$ and the x and y axes along $\langle \bar{1}10\rangle$ and $\langle 001\rangle$, respectively. For $\mathbf{H}\|[001]$, two lines are expected at g_y and at $g_{xz}=\sqrt{(g_x^2+g_z^2)/2}$ with degeneracies of 4 and 8, respectively. When $\mathbf{H}$ rotates in the (100) plane, these two lines split into three lines, and for $\mathbf{H}\|[011]$ the signal consists of lines at g_x, g_z, and $g_{xyz}=1/2(\sqrt{g_x^2+2g_y^2+g_z^2})$ with degeneracies of 2, 2, and 8, respectively. Experimentally, the orthorhombic symmetry of signal IV was difficult to verify because of the small signal intensity, especially when the external magnetic field was rotated in the (100) plane. For $\mathbf{H}\|[011]$, only one line attributed to the transition g_{xyz} (the more intense line) was observed at $g\approx1.5$ for the three materials.

B. Site I: O_h site symmetry

The weak differences between the experimental and theoretical g values for site I are attributed to crystal-field admixture between Γ_7 of the $J=5/2$ manifold and the excited state $\Gamma_{7'}$ within the $J=7/2$ manifold. We performed standard crystal-field theory calculation to further investigate the effect of crystal-field admixtures on the g factor. The calculations were based on the single-ion Hamiltonian which includes the spin-orbit coupling and the cubic crystal field for the $4f^1$ configuration ($L=3$, $S=1/2$) (Ref. 15):

$$\mathcal{H}=-\lambda\mathbf{L}\cdot\mathbf{S}+\frac{b_4}{60}(O_4^0+5O_4^4)+\frac{b_6}{180}(O_6^0-21O_6^4), \quad (1)$$

where O_m^n are the standard crystal-field operators for $L=3$, b_4 and b_6 are the crystal-field parameters,[20] and λ is the spin-orbit coupling constant $[(7/2)\lambda\approx3240\ \mathrm{K}]$.[15]

We derived to the second-order perturbation the expression for the effective g factor for the mixed ground state Γ_7^* as a function of the energy splitting between the Γ_7 and $\Gamma_{7'}$ states calculated by first-order perturbation theory $\Delta_{77'}=\frac{7}{2}\lambda-\frac{10}{7}b_4-12b_6$ and the crystal-field admixture coefficient $V_{77'}=-\frac{4\sqrt{3}}{7}(5b_4+42b_6)$. We obtained

$$g=\langle\Gamma_7^*|L_z+2S_z|\Gamma_7^*\rangle=-\frac{10}{7}-\frac{16\sqrt{3}}{21}\alpha+\frac{24}{7}\alpha^2, \quad (2)$$

where

$$\alpha=\frac{V_{77'}}{\Delta_{77'}/2+\frac{1}{2}\sqrt{\Delta_{77'}^2+V_{77'}^2}}, \quad |\Gamma_7^*\rangle=|\Gamma_7\rangle-\tfrac{V_{77'}}{\Delta_{77'}}|\Gamma_{7'}\rangle.$$

Equation (2) predicts a reduction in the g value for $\lambda\gg b_4\gg|b_6|$ with $b_4>0$. The larger shift in the g values for PbA corresponds to an increase in the crystal-field strength due to a decrease in the lattice parameters (a) from A=Te to A=S. The obtained results agree with the point-charge model predicting $b_4\propto a^{-5}$. The values of b_4 and b_6 were determined from both the experimental g values and crystal-field splitting deduced from the magnetic-susceptibility measurements.[17] These values are listed in Table I.

Some of the reduction in the g values can also be attributed to covalent bonding. For example, in the case of Yb^{3+} in $Pb_{1-x}Yb_xA$,[21] the ground state is the Γ_6 doublet of the $J=7/2$ manifold, with no crystal-field admixture from the $J=5/2$ manifold, as it does not contain a Γ_6 representation. Thus, for Yb^{3+} the small reduction in the g factor was mainly attributed to the existence of covalent bonding. The possibility of contributions from both mechanisms, covalent bonding and crystal-field admixture, was also explored for $Pb_{1-x}Ce_xA$. However, our calculations [using an orbital reduction factor k in Eq. (1)] showed that this produces an increase in the crystal-field parameters (b_4 and b_6) and a decrease in their ratio (b_4/b_6). This decrease in b_4/b_6 causes a strong deviation from the point-charge model and, consequently, the shift in the g values was mainly attributed to crystal-field admixtures.

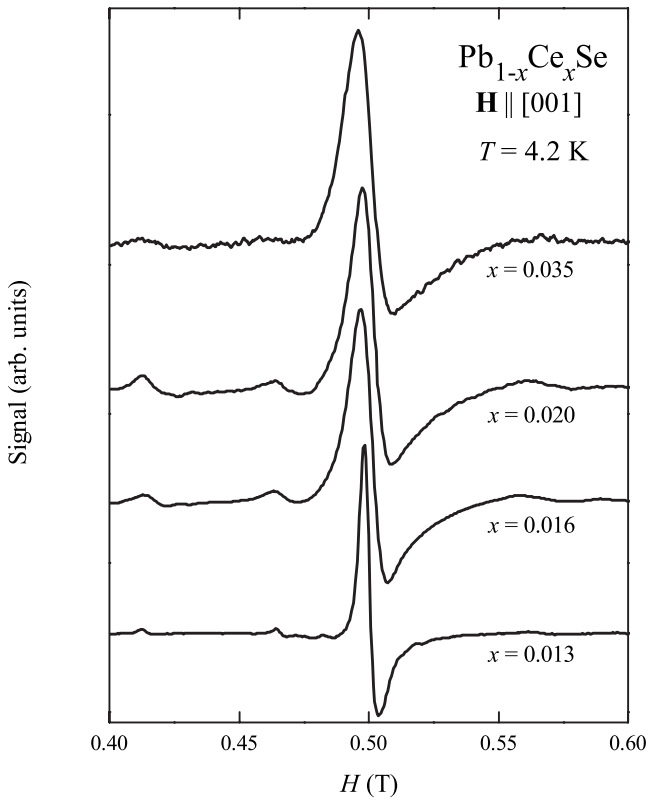

FIG. 3. Evolution of the EPR spectrum of $Pb_{1-x}Ce_xSe$ as a function of cerium concentration. The height (peak to peak) of the central signal due to Ce^{3+} ions in site I is normalized to the same value.

C. Sites II and III: Axial symmetry

The g values for sites II and III in the three DMSs are listed in Table II. These values show a clear conservation of the **g**-tensor trace ($3g \approx 2g_\perp + g_\parallel$) predicted for weak distortion of the cubic symmetry. The axial distortion of the cubic crystal field was modeled by introducing the term of axial symmetry $b_2^0 O_2^0$ in the Hamiltonian of Eq. (1). We derived the expression of the $g_\perp$ and $g_\parallel$ factors to the first order of perturbation theory as follows:

$$g_\parallel = 2g\langle\Gamma_7|J_z|\Gamma_7\rangle = g(1 + 8\beta - 171\beta^2), \tag{3a}$$

$$g_\perp = 2g\langle\Gamma_7^+|J_x|\Gamma_7^-\rangle = g(1 - 4\beta - 135\beta^2) \tag{3b}$$

with $\beta = \frac{3}{11}\frac{b_2^0}{b_4}$.

The values of b_2^0 given in Table II were determined from Eqs. (3a) and (3b) to match the experimental values of $g_\parallel$ and $g_\perp$ for sites II and III. The results were also verified by diagonalization of the perturbed Hamiltonian with $b_2^0 O_2^0$ added to Eq. (1).

D. Dependence on cerium concentration

Figure 3 shows the spectra for four samples of $Pb_{1-x}Ce_xSe$ with $x=0.013-0.035$. The EPR spectra for samples with the lowest Ce concentration $x=0.001$ and 0.003 (not shown here) are composed only by line from site I. For the samples with $x \gg 0.013$, EPR lines due to sites II, III, and IV were detected. The relative line intensities of sites II, III, and IV as compared to that of the cubic site increase with increasing Ce concentration for $x < 0.035$. An increase in the linewidth was also observed for increasing Ce concentration, which was attributed to dipolar interaction. The overall characteristics present in the $Pb_{1-x}Ce_xSe$ spectra of Fig. 3 were also observed for $Pb_{1-x}Ce_xS$ ($x=0.008$, 0.010, and 0.020). For $x=0.008$, only EPR signal due to site I is detected. However, in the case of $Pb_{1-x}Ce_xTe$, EPR signals due to cubic and noncubic sites were detected for concentrations as low as $x=0.004$ and $x=0.007$. From the analysis of the line intensities, we estimated the relative population of the various sites. It was found that, for $Pb_{0.996}Ce_{0.004}Te$, 85% of the total number of Ce^{3+} ions are in cubic site. This number was found to be larger (91%) for $Pb_{0.987}Ce_{0.013}Se$ and 94% for $Pb_{0.99}Ce_{0.01}S$. Moreover, for all the samples studied, it was found that the relative populations of sites II, III, and IV are quite similar. Figure 4 shows the ratio of the population of site III to the population of site I (labeled P_{III} hereafter). The data were obtained from the EPR intensity analysis of signals I and III. We clearly observe that the relative population P_{III} is material dependent and that for a given cerium concentration $P_{III}(PbTe) > P_{III}(PbSe) > P_{III}(PbS)$.

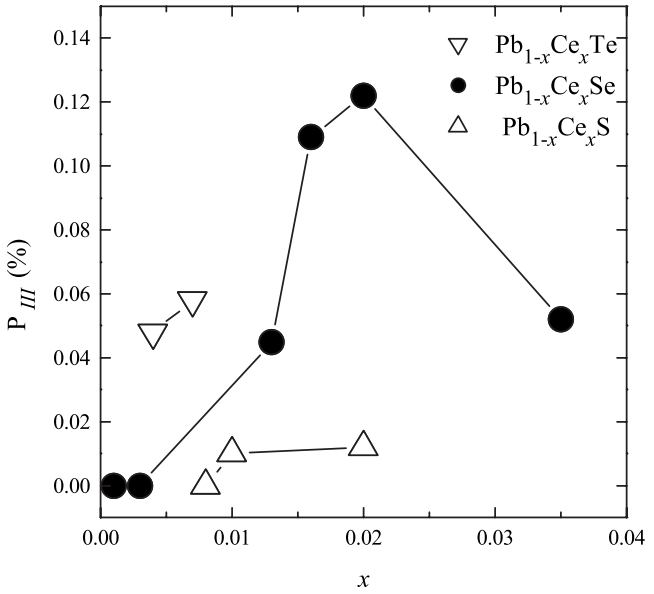

FIG. 4. Ratio of the population of site III to the population of site I for the three DMSs. The data were obtained from the EPR intensity analysis of signals.

IV. DISCUSSION

Local defects associated with dopant substitution for charge compensation are common in diluted materials.[22–24] They are cation vacancies in nn or next-nearest-neighbor (nnn) site. They can also be impurity ions in substitution sites or interstitial anions. Their presence around the magnetic ions significantly disturbs the original site symmetry. Previous results[11,24] on SrS doped with Ce^{3+} ions are in line with the present study. It was established that the axial Ce^{3+} sites were due to the existence of Sr vacancies near the Ce^{3+}

ions. Self-compensation was observed in IV-VI semiconductors doped with nonmagnetic ions.[12–14] This implies the formation of native defects with doping activity opposite to the impurities.

We attribute the existence of different site symmetries in $Pb_{1-x}Ce_xA$ to the presence of native defects near the Ce^{3+} ions which compensates its donor activity. A native defect located at a nn or nnn site of the magnetic ion should cause orthorhombic and tetragonal distortions of the cubic symmetry, respectively. A plausible native defect is a lead lattice vacancy located at a nnn position for sites II and III and at a nn position for site IV. The effect of the presence of a lead vacancy at the nnn position can be described by an axial parameter b_2^0 which is, according to a point-charge model and assuming a rigid lattice, negative and proportional to the charge of the vacancy ($Z=2$ for a neutral vacancy) and to $1/a^3$, where a is the lattice parameter. From the experiment we obtained $b_2^0(\mathrm{III})/b_2^0(\mathrm{II}) \approx 2.5$ for the three DMSs. Then we may consider a neutral vacancy for site II and a doubly negative charged vacancy for site III.

Ce^{3+} ions in the cation sublattice act as donors[25,26] giving one electron per ion to the conduction band. Thus, the carrier concentration should follow $n=N_{Ce^{3+}}$. On the other hand, lead lattice vacancies ($V_{Pb^{2+}}$) act as acceptor impurities. Assuming a complete neutrality of the cerium donor activities, one $V_{Pb^{2+}}$ would be created per two cerium ions and the electroneutrality equation can be written as $n\text{-}p=N_{Ce^{3+}}-2N_{V_{Pb^{2+}}}$.

Figure 5(a) shows the dependence of the carrier concentration $n=f(N_{Ce^{3+}})$ for $Pb_{1-x}Ce_xSe$ obtained at $T=300$ K. This dependence can be divided into two regions. At cerium concentration lower than $x=0.02$, a partial compensation of the cerium donor activity was observed with a linear dependence given by $n \approx N_{Ce^{3+}}/4$. In the second region, for $x \geq 0.02$, we observed a linear variation with a slope of 1 which indicates that in the second region, the cerium donor activity is no longer compensated. According to the scheme $N_{V_{Pb^{2+}}}=(N_{Ce^{3+}}-n/2)$, the concentration of lead vacancies is displayed as a function of x in Fig. 5(b). In the first region, two vacancies of lead are created per five Ce^{3+} ions and the limit of compensation is achieved for a lead vacancy concentration of about 1.2×10^{20} cm^{-3}. Moreover, the variation of the vacancy concentration as a function of x agrees quite well with the concentration dependence of the population of site III displayed in Fig. 4. The maximum population for site III is obtained for x near 2% where the limit of compensation is attained.

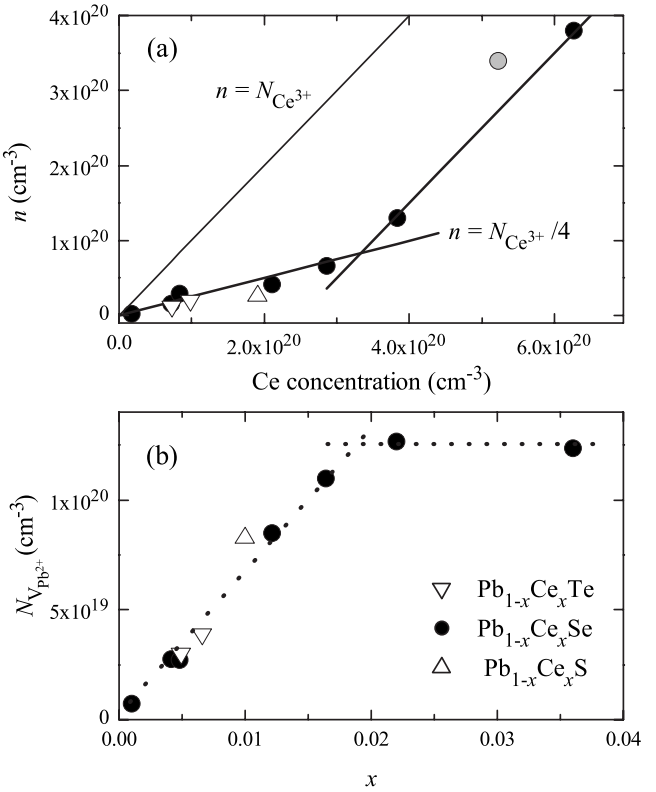

FIG. 5. (a) Carrier concentration of $Pb_{1-x}Ce_xA$ samples as a function of the Ce concentration determined at $T=300$ K. The data represented by a circle in gray color for $Pb_{1-x}Ce_xSe$ is from previous work (Ref. 27). (b) Concentration of lead vacancy as a function of x calculated from the relation $N_{V_{Pb^{2+}}}=(N_{Ce^{3+}}-n/2)$.

V. SUMMARY

The salient results of the present study are as follows:

(i) Unlike other trivalent rare-earth ions, cerium was found to be incorporated only as Ce^{3+} in the cation sublattice of lead salts compounds.

(ii) Four different types of Ce^{3+} substituting Pb^{2+} sites are present. The most populated site corresponds to that with octahedral (O_h) cubic symmetry. The existence of other types of sites was attributed to the presence of Pb vacancies acting as charge compensators near the Ce^{3+} ions.

(iii) The donor activity of Ce^{3+} ions was found to be compensated by acceptorlike Pb vacancies. The results were explained by the formation of two lead vacancies per five Ce^{3+} ions.

Furthermore, the present study may explain the existence of two types of antiferromagnetic nn Ce^{3+} pairs previously reported by magnetization steps measurements. We propose that cerium pairs with isotropic exchange interaction are due to two nn Ce^{3+} ions located into cubic sites (with no lead vacancy in the near vicinity). The other group of nn pairs is ascribed to pairs with a nearby lead vacancy affecting both strength of the exchange interaction and its anisotropy.

ACKNOWLEDGMENTS

This work was supported by FAPESP and CNPq (Brazil) and by the URB of the American University of Beirut (AUB).

[1] G. Bauer and H. Pascher, in *Diluted Magnetic Semiconductors*, edited by M. Jain (World Scientific, Singapore, 1991).
[2] See, e.g., *Semimagnetic Semiconductors and Diluted Magnetic Semiconductors*, edited by M. Averous and M. Balkanski (Plenum, New York, 1991); *Diluted Magnetic Semiconductors*, edited by J. K. Furdyna and J. Kossut, Semiconductors and Semimetals Vol. 25 (Academic, New York, 1988); T. Dietl, in *Handbook on Semiconductors*, edited by T. S. Moss (North Holland, Amsterdam, 1994), Vol. 3b, p. 1251.
[3] E. P. Skipetrov, N. A. Chernova, L. A. Skipetrova, and E. I. Slyn'ko, Mater. Sci. Eng., B **91-92**, 412 (2002).
[4] I. I. Ivanchik, D. R. Khokhlov, A. V. Morozov, A. A. Terekhov, E. I. Slyn'ko, V. I. Slyn'ko, A. de Visser, and W. D. Dobrowolski, Phys. Rev. B **61**, R14889 (2000).
[5] D. M. Zayachuk and O. A. Dobryanski, Semiconductors **32**, 1185 (1998).
[6] D. M. Zayachuk, V. I. Kempnyk, W. Bednarski, and S. Waplak, J. Magn. Magn. Mater. **191**, 207 (1999).
[7] X. Gratens, E. ter Haar, V. Bindilatti, N. F. Oliveira, Jr., Y. Shapira, and Z. Golacki, J. Magn. Magn. Mater. **226-230**, 2036 (2001).
[8] X. Gratens, V. Bindilatti, E. ter Haar, N. F. Oliveira, Jr., Y. Shapira, and Z. Golacki, Physica B **284-288**, 1519 (2000).
[9] X. Gratens, V. Bindilatti, N. F. Oliveira, Jr., and Z. Golacki, Physica B **329-333**, 1245 (2003).
[10] Y. Shapira and V. Bindilatti, J. Appl. Phys. **92**, 4155 (2002).
[11] W. Tong, L. Zhang, W. Park, M. Chaichimansour, B. K. Wagner, and C. J. Summers, Appl. Phys. Lett. **71**, 2268 (1997).
[12] S. A. Nemov, T. A. Gavrikova, V. A. Zykov, P. A. Osipov, and V. I. Proshin, Semiconductors **32**, 689 (1998).
[13] O. Nugraha, W. Tamura, O. Itoh, T. Amemiya, K. Suto, and J. Nishizawa, J. Cryst. Growth **222**, 38 (2001).
[14] V. I. Kaidanov, S. A. Nemov, and Y. I. Ravich, Semiconductors **28**, 223 (1994).
[15] A. Abragam and B. Bleaney, *Electron Paramagnetic Resonance of Transitions Metal Ions* (Oxford University Press, New York, 1970).
[16] The magnetization measurements were performed at 2 K, in magnetic fields up to 7 T using a superconducting quantum interference device (SQUID) magnetometer. The data, after a small correction for the lattice diamagnetism, were fitted to a modified Brillouin function whose saturation value yielded x. We used an effective spin $S=1/2$ and the g values of the cubic site obtained in the present work.
[17] The susceptibility data were taken from 300 to 2 K. The data were fitted by the expression of E. D. Jones, Phys. Lett. **22**, 266 (1966) which includes the effect of the crystal-field splitting and exchange interactions.
[18] P. Fita, K. Smolinski, Z. Golacki, and K. Lawniczak-Jablonska, Appl. Phys. A: Mater. Sci. Process. **68**, 681 (1999).
[19] F. J. Dyson, Phys. Rev. **98**, 349 (1955).
[20] M. T. Hutchings, in *Solid State Physics*, edited by F. Seitz and D. Turnbull (Academic, New York, 1964), Vol. 16, p. 227.
[21] S. Isber, S. Charar, X. Gratens, C. Fau, M. Averous, S. K. Misra, and Z. Golacki, Phys. Rev. B **54**, 7634 (1996).
[22] G. D. Watkins, Phys. Rev. **113**, 79 (1959).
[23] J. L. Boldú, R. J. Gleason, and M. Georgiev, Phys. Rev. B **32**, 7043 (1985).
[24] W. L. Warren, K. Vanheusden, C. H. Seager, D. R. Tallant, J. A. Tuchman, S. D. Silliman, and D. T. Brower, J. Appl. Phys. **80**, 7036 (1996).
[25] D. L. Partin, J. Appl. Phys. **57**, 1997 (1985).
[26] G. T. Alekseeva, M. V. Vedernikov, E. A. Gurieva, P. P. Konstantinov, L. V. Prokof'eva, and Yu. I. Ravich, Semiconductors **32**, 716 (1998).
[27] V. Jovovic, S. J. Thiagarajan, J. West, J. P. Heremans, T. Story, Z. Golacki, W. Paszkowicz, and V. Osinniy, J. Appl. Phys. **102**, 043707 (2007).